Environmental Science & Technology Letters

pubs.acs.org/journal/estlcu

Letter

Chemical Boundary Layer and Its Impact on Air Pollution in Northern China

Xin Huang,* Jiantao Huang, Chuanhua Ren, Jiaping Wang, Hongyue Wang, Jiandong Wang, Hao Yu, Jing Chen, Jian Gao, and Aijun Ding

Cite This: *Environ. Sci. Technol. Lett.* 2020, 7, 826–832

Read Online

ACCESS | Metrics & More | Article Recommendations | Supporting Information

ABSTRACT: Planetary boundary layer (PBL) meteorology plays a vital role in air pollution, which has drawn increasing attention due to its adverse eco-environmental impacts. Although recent observational studies suggested the vertical heterogeneity of pollutants in the PBL, the overall picture illustrating the structure of the chemistry is still not fully understood, especially for polluted regions in China. Here, wintertime observations of main gaseous and particulate pollutants together with aerosol components and ground-based lidar remote sensing, as well as model simulations, are integrated to better understand the chemical process related to PBL evolution. We find that the turbulent motion does shape chemistry stratification in the PBL, reflected especially by a steep ozone drop near the surface due to a strong titration effect. Furthermore, enhanced secondary production, like sulfate and nitrate aerosols, in the upper PBL and residual layer substantially contributes to near-surface haze pollution through vertical mixing. This work sheds more light on the chemical PBL and highlights the importance of understanding pollution with a vertical perspective.

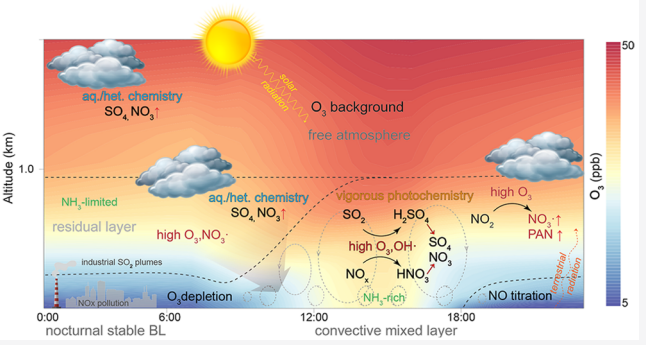

1. INTRODUCTION

The planetary boundary layer (PBL) is directly influenced by the underlying surface with a time scale of about an hour or less.[1,2] The fast response to the surface forcing makes the PBL structure quite variable in time and space.[3] Daytime solar radiation heats the surface, initiating thermal instability. As the atmosphere is warmed through turbulent mixing, rising thermals penetrate to the overlying free troposphere and give rise to a convective PBL. The daytime turbulent mixing tends to homogenize atmospheric compositions including various air pollutants that are emitted near the surface.[4] During the nighttime, the ground surface cooling due to re-emitting energy stabilizes the near-surface air, forming a nocturnal inversion with a residual layer aloft. Such a drastic diurnal change in the PBL has been demonstrated to be inherently connected to air pollution by modulating the dispersion, transport, and accumulation of pollutants.[5−7]

Air pollution causes adverse effects on human health and jeopardizes natural ecosystems.[8,9] The dispersion of pollutants that are predominantly emitted from the surface is highly dependent on PBL evolution since it defines the volume of air through which the pollution is mixed.[10,11] Many previous studies indicated that a well-developed PBL is prone to efficient dilution of pollution.[6,12] In addition to freshly emitted pollutants, nowadays, an increasingly tough pollution challenge is secondary pollutants, especially $PM_{2.5}$ (particulate matter with aerodynamic diameters less than 2.5 μm) and ozone (O_3) pollution.[13−15] These secondary pollutions are produced via photochemical processes or multiple-phase chemistry in the atmosphere,[16] and most of the reactions take place in the PBL where the gas precursors concentrate. Thus, PBL evolution greatly determines secondary pollution formation through substantially varying radiation, temperature, and water content, as well as pollutant concentrations within it.[17−19]

China has been suffering from heavy air pollution in the past decades due to fast-economic development.[20] The densely populated Beijing−Tianjin−Hebei (BTH) region features the most severe $PM_{2.5}$ pollution and also an increasing ozone level.[21−24] Some measurements in this region provided observational evidence on a strong vertical gradient for photochemical pollutants including ozone,[23,25] an increasing fraction of secondary aerosol with altitude,[26,27] and a faster formation rate of nitrate aerosol in the nocturnal residual layer.[28] Although these case studies are indicative of the vertical heterogeneity of $PM_{2.5}$ and O_3 pollution, stratification

Received: September 18, 2020
Revised: October 22, 2020
Accepted: October 22, 2020
Published: October 23, 2020

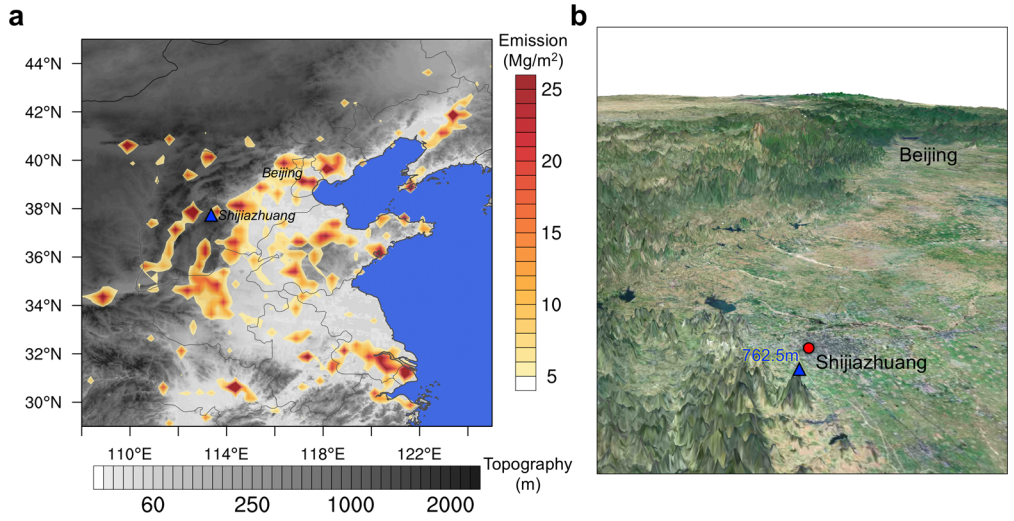

Figure 1. Study area and location of observation stations. (a) Topography and primary $PM_{2.5}$ emission. (b) Three-dimensional view of the topography in the North China Plain and geographic locations of cities and stations. The blue triangle and red dot mark the mountain station FLS and the plain station XBSY, respectively.

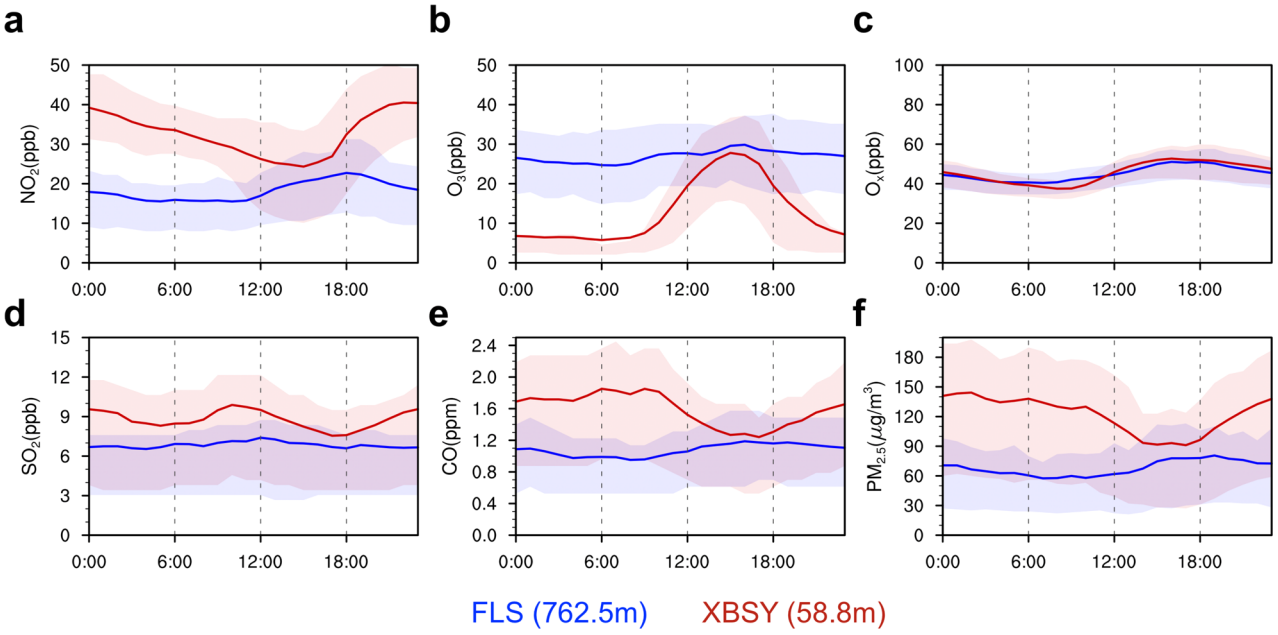

Figure 2. Distinct diurnal patterns of various air pollutants at different altitudes. (a–f) Statistical characteristics of diurnal variations of NO_2, O_3, O_x, SO_2, CO, and $PM_{2.5}$ measured at a mountain station (FLS, blue lines and shadows) and a plain station (XBSY, red lines and shadows) during the winters of 2016–2019. The solid lines present the average concentrations, and the shadows show the 25–75th percentile ranges.

of chemical processes and its interactions with PBL meteorology are still unclear. In this study, by integrating a four-year observation of air pollutants, aerosol composition measurements, ground-based lidar remote sensing, and available aircraft observation, as well as model simulations with PBL process diagnosis, we aim to provide a general picture of the chemical PBL and understand its impact on air pollution.

2. MATERIALS AND METHODS

2.1. In Situ Measurement. Hourly nitrogen dioxide (NO_2), O_3, carbon monoxide (CO), sulfur dioxide (SO_2), and $PM_{2.5}$ are measured in Shijiazhuang. Measurements of these pollutants during wintertime from 2016 to 2019 at two stations, the mountain station Fenglongshan (FLS, 114.34° E, 37.89° N) with an altitude of 762.5 m above sea level (a.s.l.), and the plain station Xibeishuiyuan (XBSY, 114.43° E, 38.17° N, 58.8 m a.s.l.) are used. The locations of the stations and emission of anthropogenic primary $PM_{2.5}$ are illustrated in Figure 1. Furthermore, aerosol components, including sulfate (SO_4^{2-}), nitrate (NO_3^-), ammonium (NH_4^+), organic matters (OM), and elemental carbon (EC), were measured by MARGA and Sunset OC-EC instrumentation in 2017 (details can be found in the Supporting Information). Additionally, lidar observations were continuously operated in Shijiazhuang during the winter of 2017, which provides vertical information on 532 nm aerosol extinction.[29]

2.2. Model Simulation and Processes Analysis. Online-coupled meteorology–chemistry simulations are conducted based on the WRF-Chem model. The simulation is conducted

https://dx.doi.org/10.1021/acs.estlett.0c00755
Environ. Sci. Technol. Lett. 2020, 7, 826–832

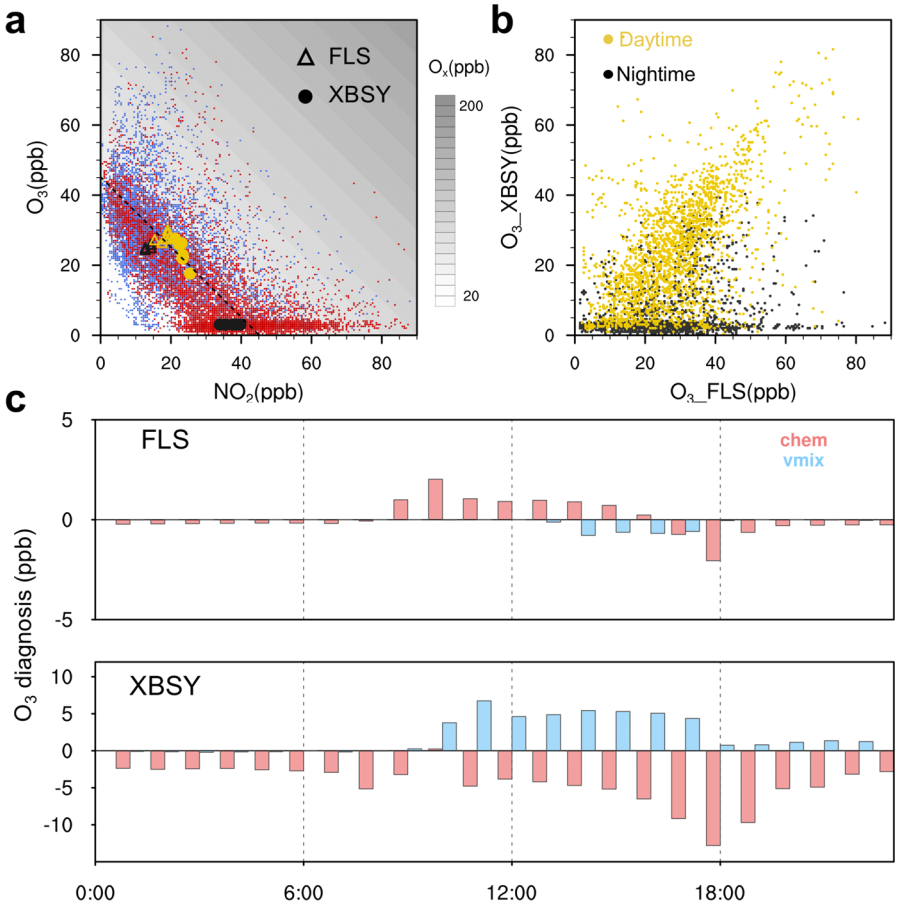

Figure 3. Ozone countergradient and the relationship with the precursors. (a) Scatter plot of NO_2 and O_3 at the mountain station FLS (blue dots) and the plain station XBSY (red dots) during the winters from 2016 to 2019. The dashed line ($x + y = 45$) shows the linear regression line for reference. Triangles and circles mark averaged hourly concentrations during daytime (golden) and nighttime (black) at these two stations. Contour background presents the O_x levels. (b) Relationship of hourly O_3 concentrations at the mountain and the plain stations. Golden and black dots present the daytime and nighttime measurements. (c) Diurnal variation of O_3 changes due to chemical production (chem) and PBL evolution (vmix) calculated from WRF-Chem analysis for the altitudes of the FLS and XBSY stations, respectively, in the winter of 2017.

from November 2017 to February 2018. To investigate the contributions of each individual physical and chemical process to variations of secondary pollutants, we performed diagnostic analysis in WRF-Chem modeling. Concentration variations induced by PBL vertical mixing and chemical transformation were diagnosed and recorded at each integration step. The information on the model simulation is detailed in the Supporting Information.

3. RESULTS AND DISCUSSION

3.1. Distinct Diurnal Characteristics at Different Altitudes. The simultaneous and long-term measurements at the mountain and plain station provide a unique insight on the air pollution at different altitudes and its possible linkage with PBL evolution. On the basis of four-year wintertime measurements during 2016−2019 with good data coverage and quality control at the two stations, the overall characteristics of diurnal cycles of main air pollutants like NO_2, O_3 ,and $PM_{2.5}$ are shown in Figure 2.

Generally, most pollutants show a lower concentration at the mountain station compared with those at the plain station due mainly to the fact that the majority of the pollutants are emitted near the ground surface. For instance, in terms of CO and NO_2, which are predominantly originated from fossil fuel combustion near the surface,[30] the averaged surface concentrations are 58% and 55% higher than the corresponding observations at the mountain station. The diurnal patterns of the surface concentrations CO and NO_2 are characterized by peak values during nighttime and reaching a minimum in the afternoon, but the observation at the mountain station FLS is exactly the opposite. It is expected that during the afternoon the turbulent mixing in the convective PBL enables vigorous updraft transport of the locally emitted pollutants, while the nocturnal stable PBL weakens the vertical dilution and accelerates the pollutant accumulation near the surface.[31] In comparison, near-surface SO_2, mainly from coal combustion in power generation and industrial production,[32] displays another peak in the early morning. Given that the smoke stack plus plume rise height often exceed several hundred meters and the countergradient of SO_2 is often observed in BTH,[32,33] the inversion breakup in the early morning tends to bring down the SO_2-concentrated plume from the previous night by entrainment and hence elevates the surface SO_2.[1,34] In BTH with densely distributed coal-fired power plants, such a morning increase of 20%−30% in near-surface SO_2 concentration further confirms the importance of the fumigation (Figure S1).

3.2. Steep Ozone Countergradient in PBL. Among all the pollutants, only O_3 features relatively higher concentrations at the mountain station FLS, with a 14 ppb (107%) increase

https://dx.doi.org/10.1021/acs.estlett.0c00755
Environ. Sci. Technol. Lett. 2020, 7, 826−832

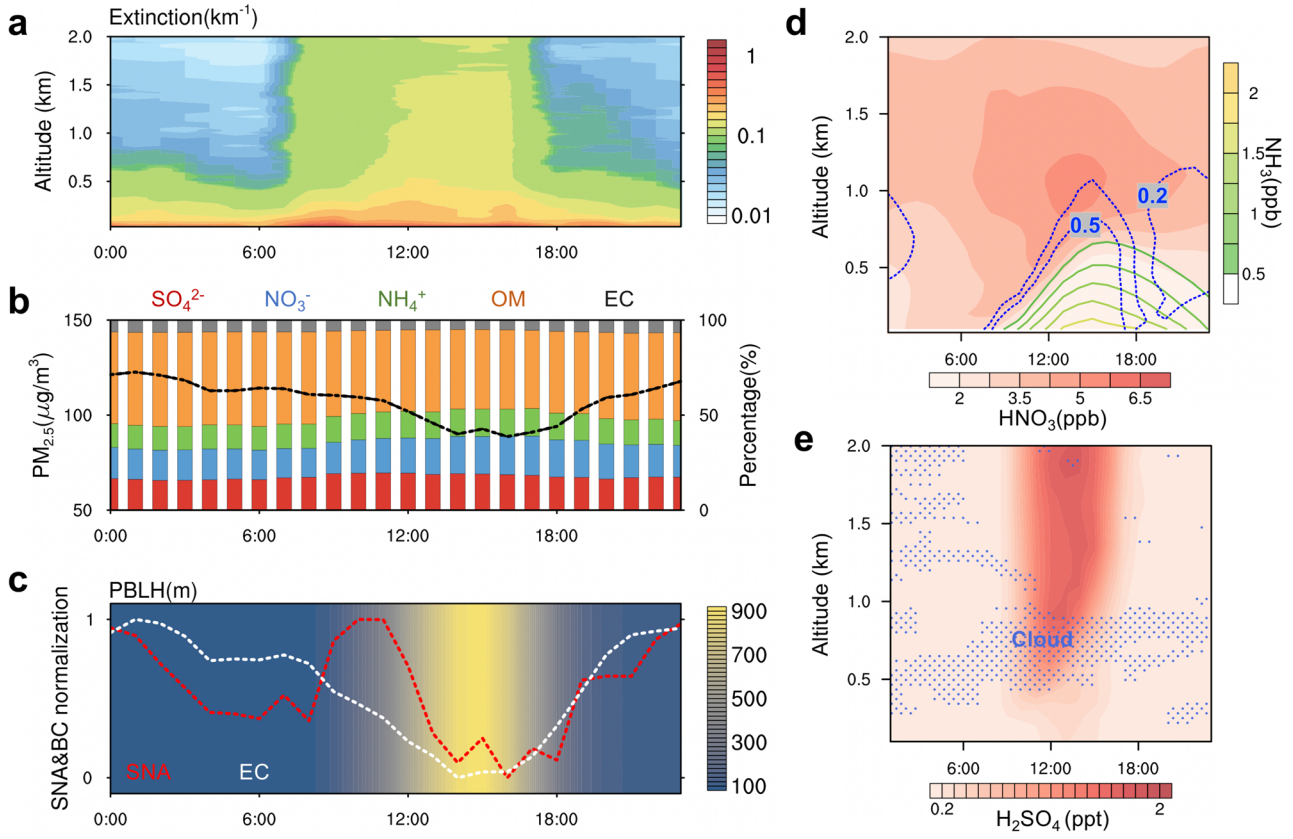

Figure 4. PBL evolution shapes the vertical structure of secondary aerosol production. (a) Diurnal pattern of median lidar-observed extinction at Shijiazhuang in the winter of 2017. (b) Diurnal pattern of $PM_{2.5}$ mass concentration and various chemical compositions, including sulfate (SO_4^{2-}), nitrate (NO_3^-), ammonium (NH_4^+), organic matter (OM), and elemental carbon (EC), at Shijiazhuang. (c) Averaged diurnal variations of SNA (SO_4^{2-} + NO_3^- + NH_4^+), EC concentration, and PBL height at Shijiazhuang in the winter of 2017. (d) Modeled vertical distributions of gaseous nitric acid (HNO_3) and ammonia (NH_3) concentration, together with chemical production of nitrate aerosol diagnosed by the WRF-Chem model (blue isolines with units of $\mu g\ m^{-3}\ h^{-1}$). (e) Vertical structure of modeled sulfuric acid (H_2SO_4) and cloud identification by lidar (blue dots, extinction greater than 5 km^{-1} and depolarization greater than 0.1) in the winter of 2017.

from the ground surface to an altitude of 762.5 m. Temporally, such a countergradient is extremely steep during midnight and the very early morning (00−08 LST), when the discrepancy could reach up to more than 20 ppb. O_3 concentrations at two stations become increasingly comparable in the afternoon since that the well-developed convective PBL tends to mix the scalars, including pollutants, uniformly vertically. Long-term aircraft measurements in the BTH region from 1995 to 2017 also confirmed an obvious O_3 countergradient in the early morning and a smaller vertical difference in the afternoon (Figure S2). Previous studies have attributed the O_3 coutergradient to two plausible mechanisms: strong NO titration effect near the surface and enhanced photochemical production in the upper air.[23,35] A quite close level of O_x (NO_2 + O_3) at the two stations throughout the day, as shown in Figure 2c, revealed that NO titration is mainly responsible for a sharp O_3 drop near the surface.

Figure 3a also indicated that O_3 and NO_2 at both stations are negatively correlated but with a constant O_x level around 45 ppb. During the daytime, O_3 concentrations at different altitudes agree very well with each other. As the night progresses, the mountain station retains the same level as that of the formerly well-mixed PBL and essentially decouples from the ground. On the contrary, the XBSY station in the surface layer features stable air with a weaker turbulence, and thus, O_3 undergoes a rapid chemical loss by reaction with locally accumulated NO. To shed more light on the relative contributions from photochemistry and PBL mixing, WRF-Chem simulations are conducted and validated by available observations (Figure S3). As shown in Figure 3c, NO titration substantially depletes O_3 near the surface, particularly after sunset, while a residual layer without direct contact with the surface keeps a higher level overnight. A residual layer exists for a while after sunrise, when solar radiation may trigger photochemical reactions and O_3 production there. As the surface continually warms, a residual layer with higher O_3 is entrained into the newly formed mixing layer and increases the near-surface O_3 level. Such an important role of PBL evolution of a morning increase in the near-surface O_3 has been observed and verified by numerical modeling in a previous work.[36]

3.3. Enhanced Secondary Aerosol Formation in Upper PBL. Although $PM_{2.5}$ pollution has been mitigated in past years, secondary aerosols are still a challenge in the winter haze in China.[37,38] As demonstrated in Figure 4, in situ measurements of aerosol chemical composition in Shijiazhuang are indicative of the dominance of secondary compositions like SO_4^{2-}, NH_4^+, and NO_3^- (SNA) in $PM_{2.5}$ concentration. In terms of the diurnal cycle, secondary aerosol SNA usually peaks before noon, differing from elemental carbon (EC) with a nighttime maximum. As a result, rising secondary aerosols and declining primary aerosols (EC and part of OM) offset each other, and hence, the $PM_{2.5}$ concentration shows little

https://dx.doi.org/10.1021/acs.estlett.0c00755
Environ. Sci. Technol. Lett. 2020, 7, 826−832

change in the morning. Vigorous turbulence in the afternoon disperses both primary and secondary aerosols into an increasingly deeper mixed layer, leading to a minimum $PM_{2.5}$ level then.

Due to the lack of observations on vertical information on aerosol chemical composition, we further analyze the vertical heterogeneity in the chemical process of secondary aerosol production with the aid of a WRF-Chem simulation. Nitrate, one important $PM_{2.5}$ composition generally with a mass contribution of more than 20%,[39,40] is mainly originated from gas-to-particle partitioning of nitric acid (HNO_3) and hydrolysis of dinitrogen-pentaoxide (N_2O_5). During the daytime, it is formed via the homogeneous gas-phase reaction between NO_2 and a hydroxyl radical (•OH) throughout the mixed layer and then neutralized by ammonia to produce ammonium nitrate (Figure 4d). Instead, at night, a nitrate radical ($•NO_3$), generated by the reaction of NO_2 with O_3, further reacts with NO_2 to establish a chemical equilibrium with N_2O_5. As aforementioned, the abundant O_3 in a residual layer could continuously react with NO_2 and efficiently produce N_2O_5.[41] At the surface, on the contrary, such a process would be greatly hindered by extremely low O_3 and high NO. Given the NO_2 profile and ammonia availability, nighttime nitrate production via gas-to-particle partitioning of nitric acid may peak at altitudes of several hundred meters. Correspondingly, the nitrate aerosol shows a notable countergradient during nighttime and early morning in the model (Figure S4). On the succeeding day, the entrainment of residual layer air into the newly formed PBL elevates the surface nitrate concentration of the nitrate aerosol, with an estimated contribution of ~60% of the morning increase. The morning peak of sulfate is attributed to a similar countergradient in SO_2 oxidation through multiple-phase chemistry. On the one hand, the atmospheric oxidizing capacity increases with height in the winter, and SO_2 itself is mainly released by elevated stacks, thereby facilitating sulfuric acid and sulfate formation in the upper PBL (Figure 4e). It is estimated by the model that SO_2 oxidation under 100 m only accounts for less than 10% of the column sulfuric acid production, while the production in the upper PBL dominates. As a result, sulfuric acid could reach up to 1.7 ppt in the upper air and is usually less than 0.2 ppt near the surface. On the other hand, winter sulfate was also significantly contributed to by cloudwater or heterogeneous chemistry. It is noteworthy that the lidar observations suggested that there usually exists a cloud layer near the capping inversion (Figure 4e),[42] which may enhance sulfate production.

3.4. Implications and Outlook. Observations of air pollutants, lidar remote sensing, and model simulations are combined to understand PBL chemical stratification in northern China. Although daily PBL evolution varies greatly due to different synoptic conditions, this work provides a general picture of the chemical PBL. We find that the turbulent motions shape pollutant stratification in the PBL. SO_2 that is mainly emitted from elevated sources tends to peak in the early morning due to fumigation. A steep countergradient is observed for ozone due mainly to strong titration near the surface. Secondary aerosol features a fast production rate in the upper PBL and residual layer. Noteworthily, aerosol in the upper PBL has been demonstrated to play an important role in modifying PBL stability, thereby deteriorating pollution accumulation.[43,44] Furthermore, upper-level aerosols influence weather/climate via mixing with light-absorbing aerosols or by serving as cloud condensation nuclei.[45] More effort on vertical chemical observation is urgently needed for better understanding of the chemical PBL and its role in air pollution and climate change.

■ ASSOCIATED CONTENT

Supporting Information

The Supporting Information is available free of charge at https://pubs.acs.org/doi/10.1021/acs.estlett.0c00755.

Detailed explanation of methods and modeling parameters employed, data quality control and model evaluation, additional results, and references (PDF)

■ AUTHOR INFORMATION

Corresponding Author

Xin Huang − *Joint International Research Laboratory of Atmospheric and Earth System Sciences, School of Atmospheric Sciences, Nanjing University, Nanjing 210023, China; Jiangsu Provincial Collaborative Innovation Center for Climate Change, Nanjing 210023, China;* orcid.org/0000-0003-0922-5014; Email: xinhuang@nju.edu.cn

Authors

Jiantao Huang − *Joint International Research Laboratory of Atmospheric and Earth System Sciences, School of Atmospheric Sciences, Nanjing University, Nanjing 210023, China; Jiangsu Provincial Collaborative Innovation Center for Climate Change, Nanjing 210023, China*

Chuanhua Ren − *Joint International Research Laboratory of Atmospheric and Earth System Sciences, School of Atmospheric Sciences, Nanjing University, Nanjing 210023, China; Jiangsu Provincial Collaborative Innovation Center for Climate Change, Nanjing 210023, China;* orcid.org/0000-0002-2606-813X

Jiaping Wang − *Joint International Research Laboratory of Atmospheric and Earth System Sciences, School of Atmospheric Sciences, Nanjing University, Nanjing 210023, China; Jiangsu Provincial Collaborative Innovation Center for Climate Change, Nanjing 210023, China*

Hongyue Wang − *Joint International Research Laboratory of Atmospheric and Earth System Sciences, School of Atmospheric Sciences, Nanjing University, Nanjing 210023, China; Jiangsu Provincial Collaborative Innovation Center for Climate Change, Nanjing 210023, China*

Jiandong Wang − *Key Laboratory for Aerosol-Cloud-Precipitation of China Meteorological Administration, School of Atmospheric Physics, Nanjing University of Information Science and Technology, Nanjing 210044, China*

Hao Yu − *Anhui Academy of Environmental Science Research, Hefei 230022, China*

Jing Chen − *Shijiazhuang Meteorological Bureau, Shijiazhuang 050081, China*

Jian Gao − *Chinese Research Academy of Environmental Sciences, Beijing 100012, China*

Aijun Ding − *Joint International Research Laboratory of Atmospheric and Earth System Sciences, School of Atmospheric Sciences, Nanjing University, Nanjing 210023, China; Jiangsu Provincial Collaborative Innovation Center for Climate Change, Nanjing 210023, China*

Complete contact information is available at: https://pubs.acs.org/10.1021/acs.estlett.0c00755

https://dx.doi.org/10.1021/acs.estlett.0c00755
Environ. Sci. Technol. Lett. 2020, 7, 826−832

Notes

The authors declare no competing financial interest.

■ ACKNOWLEDGMENTS

This work was supported by the National Natural Science Foundation of China under Grants 41875150, 41922038, and 41725020 and the Ministry of Science and Technology of the People's Republic of China (2018YFC0213800). The authors also acknowledge the support of the European Commission, Airbus, and the airlines who carry free of charge the MOZAIC equipment and perform the maintenance.

■ REFERENCES

(1) Stull, R. B. *An Introduction to Boundary Layer Meteorology*; Kluwer Academic Publishers, Dordrecht, The Netherlands, 1988; pp 2−26.
(2) LeMone, M. A.; Angevine, W. M.; Bretherton, C. S.; Chen, F.; Dudhia, J.; Fedorovich, E.; Katsaros, K. B.; Lenschow, D. H.; Mahrt, L.; Patton, E. G.; Sun, J.; Tjernstrom, M.; Weil, J. 100 Years Of Progress In Boundary-Layer Meteorology. *Meteor. Monogr.* **2019**, *59*, 9.1−9.85.
(3) Zhang, H. S.; Zhang, X. Y.; Li, Q. H.; Cai, X. H.; Fan, S. J.; Song, Y.; Hu, F.; Che, H. Z.; Quan, J. N.; Kang, L.; Zhu, T. Research Progress on Estimation of the Atmospheric Boundary Layer Height. *J. Meteorol. Res.-Prc.* **2020**, *34* (3), 482−498.
(4) Garratt, J. R. The Atmospheric Boundary-Layer - Review. *Earth-Sci. Rev.* **1994**, *37* (1−2), 89−134.
(5) Yu, H. B.; Liu, S. C.; Dickinson, R. E. Radiative effects of aerosols on the evolution of the atmospheric boundary layer. *J. Geophys. Res.* **2002**, *107*, D12.
(6) Arya, S. P. *Air Pollution Meteorology and Dispersion*; Oxford University Press, New York 1999; pp 105−124.
(7) Akimoto, H. Global air quality and pollution. *Science* **2003**, *302* (5651), 1716−1719.
(8) Yin, P.; Guo, J.; Wang, L.; Fan, W.; Lu, F.; Guo, M.; Moreno, S. B. R.; Wang, Y.; Wang, H.; Zhou, M.; Dong, Z. Higher Risk of Cardiovascular Disease Associated with Smaller Size-Fractioned Particulate Matter. *Environ. Sci. Technol. Lett.* **2020**, *7* (2), 95−101.
(9) Tie, X. X.; Huang, R. J.; Dai, W. T.; Cao, J. J.; Long, X.; Su, X. L.; Zhao, S. Y.; Wang, Q. Y.; Li, G. H. Effect of heavy haze and aerosol pollution on rice and wheat productions in China. *Sci. Rep.* **2016**, *6*, 29612.
(10) Collier, C. G.; Davies, F.; Bozier, K. E.; Holt, A. R.; Middleton, D. R.; Pearson, G. N.; Siemen, S.; Willetts, D. V.; Upton, G. J. G.; Young, R. I. Dual-Doppler lidar measurements for improving dispersion models. *Bull. Am. Meteorol. Soc.* **2005**, *86* (6), 825−838.
(11) Petaja, T.; Jarvi, L.; Kerminen, V. M.; Ding, A. J.; Sun, J. N.; Nie, W.; Kujansuu, J.; Virkkula, A.; Yang, X. Q.; Fu, C. B.; Zilitinkevich, S.; Kulmala, M. Enhanced air pollution via aerosol-boundary layer feedback in China. *Sci. Rep.* **2016**, *6*. DOI: 10.1038/srep18998
(12) Emeis, S.; Schafer, K. Remote sensing methods to investigate boundary-layer structures relevant to air pollution in cities. *Bound.-Lay. Meteorol.* **2006**, *121* (2), 377−385.
(13) Wang, T.; Xue, L. K.; Brimblecombe, P.; Lam, Y. F.; Li, L.; Zhang, L. Ozone pollution in China: A review of concentrations, meteorological influences, chemical precursors, and effects. *Sci. Total Environ.* **2017**, *575*, 1582−1596.
(14) Zhu, T. Air pollution in China: scientific challenges and policy implications. *Natl. Sci. Rev.* **2017**, *4* (6), 800−801.
(15) Mills, G.; Pleijel, H.; Malley, C. S.; Sinha, B.; Cooper, O. R.; Schultz, M. G.; Neufeld, H. S.; Simpson, D.; Sharps, K.; Feng, Z.; Gerosa, G.; Harmens, H.; Kobayashi, K.; Saxena, P.; Paoletti, E.; Sinha, V.; Xu, X. Tropospheric Ozone Assessment Report: Present-day tropospheric ozone distribution and trends relevant to vegetation. *Elem. Sci. Anth.* **2018**, *6*, 47.
(16) Seinfeld, J. H.; Pandis, S. N. *Atmospheric Chemistry and Physics: From Air Pollution to Climate Change*; John Wiley, New York, 2016; pp 69−301.
(17) Fast, J. D.; Doran, J. C.; Shaw, W. J.; Coulter, R. L.; Martin, T. J. The evolution of the boundary layer and its effect on air chemistry in the Phoenix area. *J. Geophys. Res.-Atmos.* **2000**, *105* (D18), 22833−22848.
(18) Huang, X.; Ding, A. J.; Wang, Z. L.; Ding, K.; Gao, J.; Chai, F. H.; Fu, C. B. Amplified transboundary transport of haze by aerosol-boundary layer interaction in China. *Nat. Geosci.* **2020**, *13* (6), 428−434.
(19) Sun, Y. Research advances on vertical structures of physical and chemical properties of urban boundary layer and formation mechanisms of atmospheric pollution. *Kexue Tongbao* **2018**, *63* (14), 1374−1389.
(20) Liu, F.; Zhang, Q.; Tong, D.; Zheng, B.; Li, M.; Huo, H.; He, K. B. High-resolution inventory of technologies, activities, and emissions of coal-fired power plants in China from 1990 to 2010. *Atmos. Chem. Phys.* **2015**, *15* (23), 13299−13317.
(21) Wang, L. W.; Wang, X. F.; Gu, R. R.; Wang, H.; Yao, L.; Wen, L.; Zhu, F. P.; Wang, W. H.; Xue, L. K.; Yang, L. X.; Lu, K. D.; Chen, J. M.; Wang, T.; Zhang, Y. H.; Wang, W. X. Observations of fine particulate nitrated phenols in four sites in northern China: concentrations, source apportionment, and secondary formation. *Atmos. Chem. Phys.* **2018**, *18* (6), 4349−4359.
(22) Wang, N.; Lyu, X. P.; Deng, X. J.; Huang, X.; Jiang, F.; Ding, A. J. Aggravating O3 pollution due to NOx emission control in eastern China. *Sci. Total Environ.* **2019**, *677*, 732−744.
(23) Ding, A. J.; Wang, T.; Thouret, V.; Cammas, J. P.; Nedelec, P. Tropospheric ozone climatology over Beijing: analysis of aircraft data from the MOZAIC program. *Atmos. Chem. Phys.* **2008**, *8* (1), 1−13.
(24) Huang, X.; Wang, Z. L.; Ding, A. J. Impact of Aerosol-PBL Interaction on Haze Pollution: Multiyear Observational Evidences in North China. *Geophys. Res. Lett.* **2018**, *45* (16), 8596−8603.
(25) Qiu, Y. L.; Lin, W. L.; Li, K.; Chen, L.; Yao, Q.; Tang, Y. X.; Ma, Z. Q. Vertical characteristics of peroxyacetyl nitrate (PAN) from a 250-m tower in northern China during September 2018. *Atmos. Environ.* **2019**, *213*, 55−63.
(26) Wang, Q. Q.; Sun, Y. L.; Xu, W. Q.; Du, W.; Zhou, L. B.; Tang, G. Q.; Chen, C.; Cheng, X. L.; Zhao, X. J.; Ji, D. S.; Han, T. T.; Wang, Z.; Li, J.; Wang, Z. F. Vertically resolved characteristics of air pollution during two severe winter haze episodes in urban Beijing, China. *Atmos. Chem. Phys.* **2018**, *18* (4), 2495−2509.
(27) Zhao, D. L.; Tie, X. X.; Gao, Y.; Zhang, Q.; Tian, H. J.; Bi, K.; Jin, Y. L.; Chen, P. F. In-Situ Aircraft Measurements of the Vertical Distribution of Black Carbon in the Lower Troposphere of Beijing, China, in the Spring and Summer Time. *Atmosphere* **2015**, *6* (5), 713−731.
(28) Wang, Z.; Wang, W. H.; Tham, Y. J.; Li, Q. Y.; Wang, H.; Wen, L.; Wang, X. F.; Wang, T. Fast heterogeneous N2O5 uptake and ClNO2 production in power plant and industrial plumes observed in the nocturnal residual layer over the North China Plain. *Atmos. Chem. Phys.* **2017**, *17* (20), 12361−12378.
(29) Fernald, F. G. Analysis of Atmospheric Lidar Observations - Some Comments. *Appl. Opt.* **1984**, *23* (5), 652−653.
(30) Zhang, Q.; Streets, D. G.; He, K.; Wang, Y.; Richter, A.; Burrows, J. P.; Uno, I.; Jang, C. J.; Chen, D.; Yao, Z.; Lei, Y. NOx emission trends for China, 1995−2004: The view from the ground and the view from space. *J. Geophys. Res.* **2007**, *112* (D22), na DOI: 10.1029/2007JD008684.
(31) Sun, W. Y. Air-Pollution in a Convective Boundary-Layer. *Atmos. Environ.* **1986**, *20* (10), 1877−1886.
(32) Li, M.; Zhang, Q.; Kurokawa, J.; Woo, J. H.; He, K. B.; Lu, Z. F.; Ohara, T.; Song, Y.; Streets, D. G.; Carmichael, G. R.; Cheng, Y. F.; Hong, C. P.; Huo, H.; Jiang, X. J.; Kang, S. C.; Liu, F.; Su, H.; Zheng, B. MIX: a mosaic Asian anthropogenic emission inventory under the international collaboration framework of the MICS-Asia and HTAP. *Atmos. Chem. Phys.* **2017**, *17* (2), 935−963.

(33) Wang, Y.; Dorner, S.; Donner, S.; Bohnke, S.; De Smedt, I.; Dickerson, R. R.; Dong, Z.; He, H.; Li, Z.; Li, Z.; Li, D.; Liu, D.; Ren, X. R.; Theys, N.; Wang, Y. Y.; Wang, Y.; Wang, Z. Z.; Xu, H.; Xu, J. W.; Wagner, T. Vertical profiles of NO2, SO2, HONO, HCHO, CHOCHO and aerosols derived from MAX-DOAS measurements at a rural site in the central western North China Plain and their relation to emission sources and effects of regional transport. *Atmos. Chem. Phys.* **2019**, *19* (8), 5417−5449.
(34) Deardorff, J. W.; Willis, G. E. Ground-Level Concentrations Due to Fumigation into an Entraining Mixed Layer. *Atmos. Environ.* **1982**, *16* (5), 1159−1170.
(35) Swartzendruber, P. C.; Chand, D.; Jaffe, D. A.; Smith, J.; Reidmiller, D.; Gratz, L.; Keeler, J.; Strode, S.; Jaegle, L.; Talbot, R. Vertical distribution of mercury, CO, ozone, and aerosol scattering coefficient in the Pacific Northwest during the spring 2006 INTEX-B campaign. *J. Geophys. Res.* **2008**, *113* (D10), na DOI: 10.1029/2007JD009579.
(36) Xu, Z. N.; Huang, X.; Nie, W.; Shen, Y. C.; Zheng, L. F.; Xie, Y. N.; Wang, T. Y.; Ding, K.; Liu, L. X.; Zhou, D. R.; Qi, X. M.; Ding, A. J. Impact of Biomass Burning and Vertical Mixing of Residual-Layer Aged Plumes on Ozone in the Yangtze River Delta, China: A Tethered-Balloon Measurement and Modeling Study of a Multiday Ozone Episode. *J. Geophys. Res.-Atmos.* **2018**, *123* (20), 11786−11803.
(37) Ding, A. J.; Huang, X.; Nie, W.; Chi, X. G.; Xu, Z.; Zheng, L. F.; Xu, Z. N.; Xie, Y. N.; Qi, X. M.; Shen, Y. C.; Sun, P.; Wang, J. P.; Wang, L.; Sun, J. N.; Yang, X. Q.; Qin, W.; Zhang, X. Z.; Cheng, W.; Liu, W. J.; Pan, L. B.; Fu, C. B. Significant reduction of PM2.5 in eastern China due to regional-scale emission control: evidence from SORPES in 2011−2018. *Atmos. Chem. Phys.* **2019**, *19* (18), 11791−11801.
(38) Sun, Y. L.; Wang, Z. F.; Du, W.; Zhang, Q.; Wang, Q. Q.; Fu, P. Q.; Pan, X. L.; Li, J.; Jayne, J.; Worsnop, D. R. Long-term real-time measurements of aerosol particle composition in Beijing, China: seasonal variations, meteorological effects, and source analysis. *Atmos. Chem. Phys.* **2015**, *15* (17), 10149−10165.
(39) Huang, X.; Song, Y.; Zhao, C.; Li, M. M.; Zhu, T.; Zhang, Q.; Zhang, X. Y. Pathways of sulfate enhancement by natural and anthropogenic mineral aerosols in China. *J. Geophys. Res.-Atmos.* **2014**, *119* (24), 14165−14179.
(40) Sun, P.; Nie, W.; Chi, X. G.; Xie, Y. N.; Huang, X.; Xu, Z.; Qi, X. M.; Xu, Z. N.; Wang, L.; Wang, T. Y.; Zhang, Q.; Ding, A. J. Two years of online measurement of fine particulate nitrate in the western Yangtze River Delta: influences of thermodynamics and N2O5 hydrolysis. *Atmos. Chem. Phys.* **2018**, *18* (23), 17177−17190.
(41) Brown, S. S.; Dube, W. P.; Osthoff, H. D.; Wolfe, D. E.; Angevine, W. M.; Ravishankara, A. R. High resolution vertical distributions of NO3 and N2O5 through the nocturnal boundary layer. *Atmos. Chem. Phys.* **2007**, *7*, 139−149.
(42) Zhou, C.; Yang, P.; Dessler, A. E.; Hu, Y. X.; Baum, B. A. Study of Horizontally Oriented Ice Crystals with CALIPSO Observations and Comparison with Monte Carlo Radiative Transfer Simulations. *J. Appl. Meteorol. Clim.* **2012**, *51* (7), 1426−1439.
(43) Ding, A. J.; Huang, X.; Nie, W.; Sun, J. N.; Kerminen, V. M.; Petaja, T.; Su, H.; Cheng, Y. F.; Yang, X. Q.; Wang, M. H.; Chi, X. G.; Wang, J. P.; Virkkula, A.; Guo, W. D.; Yuan, J.; Wang, S. Y.; Zhang, R. J.; Wu, Y. F.; Song, Y.; Zhu, T.; Zilitinkevich, S.; Kulmala, M.; Fu, C. B. Enhanced haze pollution by black carbon in megacities in China. *Geophys. Res. Lett.* **2016**, *43* (6), 2873−2879.
(44) Li, Z. Q.; Guo, J. P.; Ding, A. J.; Liao, H.; Liu, J. J.; Sun, Y. L.; Wang, T. J.; Xue, H. W.; Zhang, H. S.; Zhu, B. Aerosol and boundary-layer interactions and impact on air quality. *Natl. Sci. Rev.* **2017**, *4* (6), 810−833.
(45) Wang, Z. L.; Huang, X.; Ding, A. J. Dome effect of black carbon and its key influencing factors: a one-dimensional modelling study. *Atmos. Chem. Phys.* **2018**, *18* (4), 2821−2834.

https://dx.doi.org/10.1021/acs.estlett.0c00755
Environ. Sci. Technol. Lett. 2020, 7, 826−832